Soft Matter

PAPER

View Article Online
View Journal | View Issue

Cite this: *Soft Matter*, 2025, 21, 1895

Modulating melting points in micellar cores: influence of the corona chain length on the core confinement in binary mixed block copolymer micelles†

Szymon Mikołaj Szostak, [a] Nico König,[a] Lutz Willner [b] and Reidar Lund *[a]

Self-assembly of polymers with crystallizable blocks may lead to micelles with ordered, gel-like or crystalline cores. Here we investigate binary mixtures of *n*-alkyl-poly(ethylene oxide), C_n-PEO*x* (*n* = 28, *x* = 3–20 kDa) and study their self-assembly to gain insight into the effect of confinement on the core-crystallization and micellar structure. By employing identical core block length but varying corona block lengths, the size of the core can be tuned by variation of the block ratios. The micelles were characterized by small-angle X-ray scattering (SAXS) to gain insight into the overall and internal structure, including aggregation number, core size, and density distribution of the corona. SAXS curves from examined samples showed a characteristic pattern of spherical core–shell micelles but with broader corona distribution in the binary mixtures as compared to the neat samples. The structural parameters of the micelles were extracted from the SAXS data by employing a spherical core–shell model with dual density profiles in the core. We found that the aggregation number decreases as PEO length increases following a power law predicted in the literature. Furthermore, the melting point and melting enthalpy of crystalline alkyl cores were closely inspected by densitometry and differential scanning calorimetry (DSC). Correlating the core radius obtained from SAXS, we found that the melting point depression caused by the self-confinement in the micellar core can be described by the Gibbs–Thomson equation. These results show that the micellar structure and phase transition of the semicrystalline core can be easily tuned through blending diblock copolymers with different corona block lengths.

Received 5th November 2024,
Accepted 6th February 2025

DOI: 10.1039/d4sm01303d

rsc.li/soft-matter-journal

1. Introduction

The self-assembly of amphiphilic block copolymers in aqueous solution to form micellar nanoparticles has been one of the most extensively studied topics in colloidal science.[1,2] A growing number of potential biomedical applications, particularly drug delivery,[3–5] highlights the demand for structural information at nano resolution,[6,7] which combines with the corresponding performance from biological assessments to help establish the structure–property relationships.

Micelles designed for *in vivo* use need to be tested in a mimetic biological milieu, which generally means aqueous solutions. In this context, small-angle X-ray scattering (SAXS) is a powerful tool to determine the shape, size, size distribution, and internal structure of self-assembling systems in aqueous environments.[8,9] SAXS is capable of delivering structural information of dimensions between 1 and 100 nm by quantifying electron density differences at the nanoscale. Through variation of the molecular composition, molecular weight, and solvent, the nature and strength of intermolecular forces and consequently the self-assembled structures can be varied, *i.e.* in a bottom-up strategy.[10,11]

N-Alkyl-poly(ethylene oxide) (C_n-PEO), a class of relatively simple but important amphiphilic diblock copolymers, can self-assemble into micelles of core–shell structure in water with a semicrystalline alkyl core and a hydrated PEO corona. This micellar system can be used as a model system due to its simplicity and low polydispersity. We previously found that the aggregation number increased quadratically with the alkyl block length and decreased in a power-law dependence with an exponent of −0.51 on the PEO block length for single-component C_n-PEO micelles,[12] showing that the micellar structure can be tuned by varying the core and corona block lengths. Blending block copolymers of different lengths, on the other hand, represents a handy and efficient way to alter the micellar

[a] *Department of Chemistry, University of Oslo, NO-0315 Oslo, Norway. E-mail: reidar.lund@kjemi.uio.no*
[b] *Centre for Neutron Science (JCNS-1), Forschungszentrum Jülich GmbH, 52425 Jülich, Germany*

† Electronic supplementary information (ESI) available. See DOI: https://doi.org/10.1039/d4sm01303d

structure.[13–18] Recently, we systematically investigated binary mixed micelles formed by blending C_n-PEO with various alkyl block lengths at constant PEO block length and observed that the mixed micelles exhibited structural properties that perfectly interpolate those of single-component micelles.[19] However, it has not been investigated how mixed PEO block lengths will affect the structural parameters of the equilibrium micelles at a fixed alkyl block length. For commonly used hydrophobic blocks of amphiphilic diblock copolymers, *e.g.* polycaprolactone, poly(L-lactide), being semicrystalline, core crystallization is a well-known determinant factor to the microstructure[20,21] and equilibrium exchange kinetics of the formed micelles,[22,23] thereby affecting the loading capacity and stability of the micelles in drug delivery.[24] For micellar systems with crystalline cores, the temperature can be used as an external stimulus to control the melting-crystallization phase transition in the core, which enables control of the drug release mode.[25–27] For instance, upon heating through responsive co-loaded cargo or directly raising the temperature, crystalline cores transiting to the molten state can potentially make the loaded drug release faster.[28] Our previous study on C_n-PEO micelles[29] showed that the crystalline core exhibits a melting point depression that can be satisfactorily described by the Gibbs–Thomson equation. Thus this soft self-confined structure follows the same behaviour as hard confined systems such as ordinary liquids in mesoscopic pores.[30] Further research showed that the mixed micelles formed by binary mixtures of C_n-PEO with various alkyl block lengths also nicely followed the Gibbs–Thomson law, similar to the single-component counterpart although the melting points are additionally affected by the mixing of components in the core.[19] One intriguing approach to alter the core confinement is to utilise C_n-PEO*x* polymers with binary corona block length mixtures, thereby modulating the confinement and corresponding melting points.

In the present work, we address the effects of binary corona block lengths on the micellar structure and core crystallization using mixed micelles from blends of C_{28}-PEO*x* polymers with different PEO lengths (MW ranging from ~3 kDa to ~20 kDa) at various ratios. Given that the alkyl block is monodisperse and the PEO blocks synthesized by controlled anionic polymerization also exhibit very low polydispersity ($M_w/M_n \leq 1.05$), this system is well suited for assessing the effects of the corona block length. The mixed micelles were prepared *via* a co-solvent protocol. SAXS was employed to determine the structural parameters. Differential scanning calorimetry (DSC) and densitometry were carried out to observe the phase transition of the alkyl core influenced by the blending protocol.

2. Experimental

2.1 Polymer synthesis and characterization

Poly(ethylene oxide)-mono-*n*-alkyl ethers (poly(ethylene oxide)-mono-*n*-octacosyl ether), C_{28}-PEO*x* (x = 3, 5, 10, 20 kg mol^{-1}), were synthesized by living anionic ring-opening polymerization as reported in our previous work.[12] In brief, 1-octacosanol ($C_{28}H_{57}OH$) was mixed in a ratio of 80 : 20 with its corresponding potassium-1-alkoxide ($C_{28}H_{57}O^-K^+$) functioning as the initiator. The polymerizations were carried out in toluene at 95 °C under high vacuum. The molecular weight and polydispersity of the resulting polymers were determined by size exclusion chromatography (SEC) and the results are shown in Table 1.

Table 1 Weight-average molecular weight M_w in g mol^{-1}, polydispersity index M_w/M_n, and the corresponding number of repeat units N^*_{PEO} of C_{28}-PEO*x* polymers

Polymer code	M_w	M_w/M_n	N^*_{PEO}
C_{28}-PEO3	2700	1.04	53
C_{28}-PEO5	5000	1.04	105
C_{28}-PEO10	10 000	1.02	218
C_{28}-PEO20	21 800	1.05	485

2.2 Sample preparation

Single-component micelles as reference were prepared by dissolving dry C_{28}-PEO*x* copolymer powder in degassed Millipore Type I water to make a 5 mg mL^{-1} solution. The solutions were heated and shaken at 60 °C for 4 hours to ensure equilibrium. Then the solutions were cooled down to room temperature overnight while being continually shaken. For binary mixed micelles, mixtures of C_{28}-PEO*x* with two different PEO lengths in desired ratios were first dissolved in chloroform (a good solvent for both blocks) to achieve homogeneous mixing. The solvent was then removed under nitrogen flow and a series of dry homogeneous polymer blends was obtained. These blends were then dissolved in water and processed as in the above-mentioned procedures for the pure micelles.

There are seven mixed samples named with the following nomenclature: C_{28}-PEO3/5 1 : 1 denotes a mixture of C_{28}-PEO3 and C_{28}-PEO5 in a mass ratio of 1 : 1, C_{28}-PEO5/20 1 : 4 denotes a mixture of C_{28}-PEO5 and C_{28}-PEO20 in a mass ratio of 1 : 4, *etc.* For SAXS measurements at BM29 samples were diluted to concentration 2.5 mg mL^{-1} or 1.25 mg mL^{-1} to prevent radiation damage.

2.3 Density measurements

Polymer density in solution was measured with an Anton Paar DMA 5001 density meter. The densities of water, PEO, and micelle solutions were measured in a temperature range from 15 to 65 °C at a heating rate of 0.25 °C min^{-1}. The average density of the copolymer ρ_{pol} in aqueous solution was calculated based on the water density ρ_{H_2O}, the solution density ρ_{pol}, the mass of the polymer m_{pol}, the mass of water m_{H_2O}, polymer mass fraction $\chi_{pol} = \frac{m_{pol}}{m_{pol} + m_{H_2O}}$ using the following equation:

$$\rho_{pol} = \frac{\chi_{pol} \cdot \rho_{sol} \cdot \rho_{H_2O}}{\rho_{H_2O} + (\chi_{pol} - 1) \cdot \rho_{sol}} \quad (1)$$

2.4 Differential scanning calorimetry (DSC)

The melting/freezing point T_m/T_f and the melting/freezing enthalpy $\Delta H_m/\Delta H_f$ were determined by DSC. In detail, the heat capacity during heating or cooling runs was measured with a Nano DSC device (TA Instruments) at a polymer concentration

of ~5 mg mL^{-1} and a scan rate of 2 °C min^{-1} from 15 °C to 75 °C and 75 °C to 15 °C. Samples were measured in heat-cool–heat-cool mode, the data were baseline-corrected by subtracting the contribution of solvent (water) using the NanoAnalyze Software (TA Instrument). T_m/T_f was determined from the maximum peak temperature and $\Delta H_m/\Delta H_f$ was determined from the integral area of the transition peak in the heat capacity curves from the second heat-cool run.

2.5 Small angle X-ray scattering (SAXS) experiments

SAXS measurements were conducted at beamline BM29 at the European Synchrotron Radiation Facility in Grenoble, France[31] and on a Bruker NanoStar instrument (RECX, University of Oslo, Norway). A photon wavelength of λ = 1 Å (BM29) and λ = 1.54 Å (NanoStar) was used. The scattering intensity was recorded as a function of the wave vector defined as $Q = \frac{4\pi \cdot \sin(\theta)}{\lambda}$ with the scattering angle 2θ, at the polymer concentration of ~5 mg mL^{-1}. The available Q vector range varies from 0.006–0.5 Å^{-1} (BM29) to 0.01–0.3 Å^{-1} (NanoStar). The scattering intensity was corrected by subtracting the scattering contributions from the water and the empty cell and normalized to the absolute intensity with water. Measurements at BM29 were performed using an autosampler at 20 °C, the exposure was split into 10 frames lasting 1 s to avoid radiation damage and averaged if no systematic deviation was detected. Water was measured before and after the sample and averaged. Temperature SAXS measurements were performed at NanoStar, with measurement time 3600 s, heating rate between measurements 5 °C min^{-1} + 1800 s equilibration time, temperatures $T \in \{20; 30; 40; 45; 50; 55; 60\}$

2.6 Scattering model

The data were analyzed by fitting model for core–shell micelles.[12,19] In a preceding publication on C_n-PEO micelles,[32] it was established that the micellar core assumes a prolate ellipsoid configuration with an axial ratio of $\epsilon \sim 0.5$ below the melting temperature, subsequently converting into a more spherical conformation with an axial ratio of $\epsilon \sim 0.7$ above the melting point. Additionally, the core is surrounded by a thin layer of dehydrated PEO. The study implemented small angle neutron scattering (SANS) with contrast matching of the PEO chains to isolate the signal from the micellar core. In the present case, where SAXS is the sole method of analysis, determination of the core shape is precluded by the overlap of the signal at large Q with other scattering contributions from the shell. In order to circumvent overparameterization, we have assumed monodispersity of the micelles, spherical alkyl core shape and uniform hydration of PEO chain. Consequently, the core radius is to be regarded as an average radius.

In the scattering model the core consisting of alkyl chains is considered to be homogenous, solvent-free sphere of a radius R_c with scattering amplitude

$$A_c = \frac{3 \cdot \sin(Q \cdot R_c) - (Q \cdot R_c) \cdot \cos(Q \cdot R_c)}{(Q \cdot R_c)^3} \quad (2)$$

Scattering contribution from the corona is described with the following formula

$$A_s = \frac{1}{C}\int_{R_c}^{\infty} 4\pi r^2 n(r) \frac{\sin Qr}{Qr} dr \quad (3)$$

with normalization constant C described as

$$C = N_{agg} \cdot V_s \Big/ \int_{R_c}^{\infty} 4\pi r^2 n(r) dr \quad (4)$$

where V_s is the average molecular volume of the corona forming polymer calculated by:

$$V_s = V_{s1} \cdot f_{short} + V_{s2} \cdot (1 - f_{short}) \quad (5)$$

where f_{short} is the mole fraction of the short chain.

The radial density distribution function for the corona was chosen to have the following form:

$$n(r) = \frac{C}{V_s}\left[f_{short} \cdot V_{s,1} \frac{r^{-\frac{4}{3}}}{1 + \exp\frac{r - R_{m,1}}{\sigma_{out,1} R_{m,1}}} + (1 - f_{short}) \times V_{s,2} \frac{r^{-\frac{4}{3}}}{1 + \exp\frac{r - R_{m,2}}{\sigma_{out,2} R_{m,2}}} \right] \quad (6)$$

Here we assumed that each corona forming polymer follow the characteristic density profile of star-like micelles, $n(r) \sim r^{-4/3}$, $R_{m,1}$ is the characteristic radius of the shorter chains, $R_{m,2}$ and that of the longer chains which defines the outer micellar radius.

In addition, the blob scattering, originating from the corona chain scattering was calculated using[33,34]

$$B(Q) = \frac{P_{Beau}(Q)}{1 + \nu P_{Beau}(Q)} \quad (7)$$

in which ν is an effective concentration-dependent excluded-volume interaction parameter, and $P_{Beau}(Q)$ is the Beaucage form factor defined by the radius of gyration, R_g, and the fractal dimension of the chain, d_f.[34] For simplicity and lack of sensitivity, we used a common, mean R_g to represent both coronal chain. The scattering contributions were weighted by adequate contrast factors and the individual scattering contributions:

$$I_c(Q) = (\rho_c - \rho_0)^2 N_{agg}{}^2 V_c{}^2 A_c(Q)^2 \quad (8)$$

$$I_s(Q) = (\rho_s - \rho_0)^2 N_{agg}\left(N_{agg} - \frac{1}{1+\upsilon}\right) V_s{}^2 A_s(Q)^2 \quad (9)$$

$$I_{cross}(Q) = 2(\rho_s - \rho_0)(\rho_c - \rho_0) N_{agg}{}^2 V_s V_c A_s(Q) A_c(Q) \quad (10)$$

$$I_{blob}(Q) = (\rho_s - \rho_0)^2 N_{agg} V_s{}^2 B(Q) \quad (11)$$

where N_{agg} is aggregation number of micelle, V_c molecular volume of a core, and $\rho_{c/s/0}$ is scattering length density of core/shell/solvent. The final differential scattering cross section

is given by:

$$\frac{d\Sigma}{d\Omega}(Q) = \frac{\phi}{N_{agg}(V_c + V_s)}[(I_c(Q) + I_s(Q) + I_{cross}(Q))S(Q) + I_{blob}(Q)] \quad (12)$$

where ϕ is the volume fraction and $S(Q)$ is a hard-sphere structure factor which for dilute is approximately 1.[35] In the model majority of the parameters were determined by independent methods or were dependent on sample composition, the free fit parameters were the aggregation number N_{agg}, inner and outer micelle radius $R_{m,1}$ and $R_{m,2}$, ν and ρ_c. Molecular volumes were calculated from the molecular weight and density, scattering length densities were calculated from molecular volume and atomic composition, the core radius was calculated assuming spherical shape by

$$R_c = \left(\frac{3N_{agg}V_c}{4\pi}\right)^{1/3} \quad (13)$$

3. Results and discussion

3.1 Confirming the formation of binary mixed micelles

First, we hypothesize the formation of mixed micelles instead of a simple mixture of two single-component micelle populations. To assess this, we compare the SAXS curves obtained from mixtures with the fractional mass-weighted linear combinations of measured scattering data of the individual components at 20 °C. If they coincide, there is no intermixing between the two components. Instead, two populations of single-component micelles form independently. In contrast, a deviation between the two curves indicates that mixed micelles containing both component copolymers are formed. The SAXS profile of C_{28}-PEO3/20 1 : 7 was selected as a representative example, where the difference in PEO block lengths is the largest between all samples. As shown in Fig. 1a, the experimental data of C_{28}-PEO3/20 1 : 7 and the linear combination of scattering intensities from C_{28}-PEO3 and C_{28}-PEO20 do not superpose, which confirms our hypothesis.

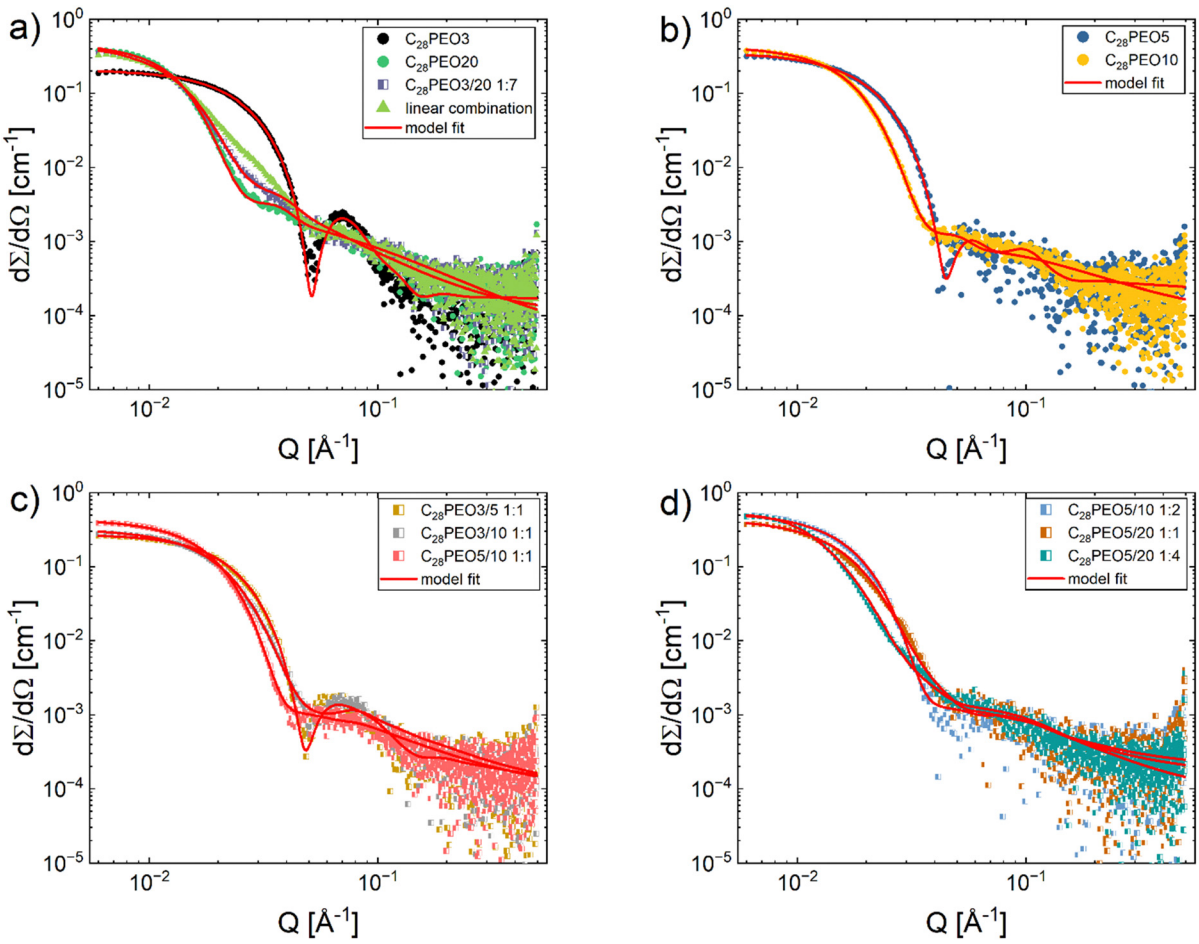

Fig. 1 (a) SAXS data of C_{28}-PEO3, C_{28}-PEO20, C_{28}-PEO3/20 1 : 7 premixed blend and the corresponding mass-weighted linear combination of C_{28}-PEO3 and C_{28}-PEO20, (b) SAXS data of samples C_{28}-PEO5, C_{28}-PEO10, (c) SAXS data of mixtures C_{28}-PEO3/5 1 : 1, C_{28}-PEO3/10 1 : 1 and C_{28}-PEO5/10 1 : 1, (d) SAXS data of mixtures C_{28}-PEO5/10 1 : 2, C_{28}-PEO5/20 1 : 1 and C_{28}-PEO5/20 1 : 4. All spectra were measured at 20 °C at BM29. Samples C_{28}-PEO5, C_{28}-PEO5/10 1 : 2 and C_{28}-PEO5/20 1 : 1 were measured at 0.125% volume fraction and data scaled to 0.25% due to observed high radiation damage at higher concentrations. The solid lines represent the best fit with a spherical core-dual shell model described in Section 2.6.

However, an analogous system of mixed C_{18}-PEOx micelles was reported to segregate into single-component micelles at a low temperature, *i.e.*, below the freezing point of the C_{18} chains. The was interpreted as the discrepancy in freezing temperatures of the C_{18} core blocks of the two copolymers.[36] Yet, Vuorte *et al.* could not reproduce the effect in coarse-grained molecular simulations. They observed a tendency for an uneven distribution of the two copolymers in the micelles, but no clearly distinct populations. It has to be noted, though, that the phase transition of the alkyl chains – which Plazzotta *et al.* cite as the cause of the segregation – cannot be emulated in their computational model.[37] In contrast, our present study focuses on a longer C_{28} alkyl chain which showed a different behavior at 20 °C, well below the melting point (will be shown in the following). At this temperature, C_{28} blocks are semi-crystalline, yet we still observed mixed micelles. This might be due to the use of longer alkyl chain as well as the entropic gain arising from mixing PEO corona blocks in terms of thermodynamics.

3.2 Extracting the micellar density profile and corona conformation

Fig. 1 shows the SAXS profiles of binary mixed micelles and single-component micelles in water (polymer volume fraction 0.25 vol%) measured at 20 °C. SAXS curves of all samples have characteristic features of spherical micelles: a high intensity at low Q, a steep intensity decay at intermediate Q, and a slowly decaying weak intensity at high Q. Detailed structural parameters were obtained by fitting the data using the spherical core-dual shell model presented in Section 2.6. The best fits are depicted with solid lines in Fig. 1, and the key structural parameters are summarized in Table 2. Effects of the mean number of ethylene oxide repeat units N^*_{PEO} on structural properties will be discussed later. A list of all structural parameters determined for all the samples is presented in Table S1 (ESI†) (BM29 data) and Table S2 (ESI†) (NanoStar data) in ESI.† Additionally, after the determination of structural parameters, we calculated the density profiles for all micelles, showing the changes in the convoluted density of the core and shell depending on the distance from the center of the micelle. We could observe the general trend of the decrease in core diameter as the PEO chain length increased. If we compare the same polymer C_{28}-PEO5 in different mixed micelles (Fig. 2) we observe the decrease in the density of the micellar shell at the border between core and shell when N^*_{PEO} increases. When we look closely at the micelles C_{28}-PEO5 and C_{28}-PEO 3/5 1 : 1 that exhibit the same outer radius, we observe that mixed micelles are more compressed close to the micellar core, whereas PEO chains in pure micelles are more stretched and have a higher density close to the micellar surface. The density profiles for samples C_{28}-PEO5, C_{28}-PEO 3/5 1 : 1, C_{28}-PEO 5/10 1 : 1 and C_{28}-PEO 5/20 1 : 1 are presented in Fig. 2, density profiles for sample C_{28}-PEO 3/10 1 : 1 at different temperatures are presented in Fig. 3b, whereas other density profiles are presented in Fig. S1 (ESI†).

Table 2 The mean number of repeat units in the PEO block N^*_{PEO} of each sample and the most important structure parameters extracted from SAXS spectra using model fit analysis

Sample	N^*_{PEO}	N_{agg}	$R_{m,1}$ [Å]	$R_{m,2}$ [Å]	R_c [Å]	D_1 [Å]	D_2 [Å]	D [Å]
C_{28}-PEO3	53	150	88		29			59
C_{28}-PEO3/5 1 : 1	72	147	84	115	29	55	31	86
C_{28}-PEO3/10 1 : 1	89	129	82	142	28	54	60	114
C_{28}-PEO5	105	111	115		27			88
C_{28}-PEO5/10 1 : 1	143	111	132	151	26	106	19	125
C_{28}-PEO5/10 1 : 2	162	116	140	162	27	113	22	135
C_{28}-PEO5/20 1 : 1	177	88	108	185	24	84	77	161
C_{28}-PEO10	218	73	164		23			141
C_{28}-PEO3/20 1 : 7	256	69	119	220	22	97	101	198
C_{28}-PEO5/20 1 : 4	288	77	100	195	23	77	95	172
C_{28}-PEO20	485	42	229		19			210

Note: $R_{m,1}$ – inner micelle radius, $R_{m,2}$ – outer micelle radius, R_c – C_{28} core radius, D_1 – thickness of inner PEO shell, $D_1 = R_{m,1} - R_c$, D_2 – thickness of outer PEO shell, $D_2 = R_{m,2} - R_{m,1}$, D – thickness of PEO shell, $D = R_{m,2} - R_c$.

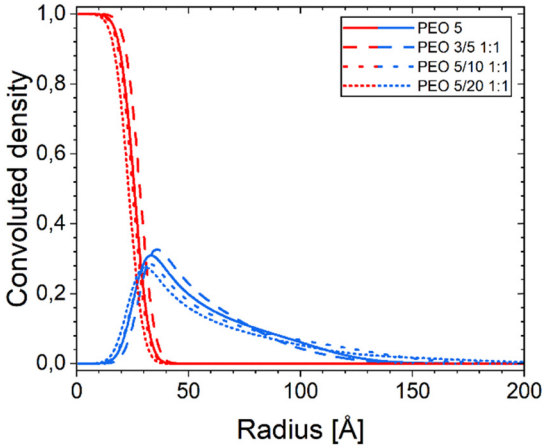

Fig. 2 Density profiles of the micelles of C_{28}-PEO5 in one-component and mixed micelles, red line denotes core density, blue line denotes shell density.

We also investigated the structure at various temperatures in the range of 20–60 °C. Representative scattering profiles of the C_{28}-PEO3/10 1 : 1 sample are displayed in Fig. 3a with corresponding density profiles presented in Fig. 3b. The scattering intensity at low Q slightly decreased with increasing temperature, which can be attributed to the change of density of the PEO blocks and water and thereby loss in contrast. The micelles maintained a spherical shape reflected in the features of SAXS curves over the tested temperatures. We also observed an abrupt increase in intensity at intermediate Q between 50 and 55 °C, indicating a significant decrease in core electron density. This phenomenon was also found in our previous works on the C_n-PEO micelle system.[19,29] Note that a sudden change in density is an implication of a first-order phase transition. Scattering curves of all other samples presented in Fig. S2 and S3 (ESI†) show a similar intensity dependence on temperature. The behavior of phase transition will be further elucidated later in the manuscript.

3.3 Effects of mixed PEO block length on micellar structure

The self-assembly of block copolymers and other macromolecules in solution is regulated both by thermodynamic and

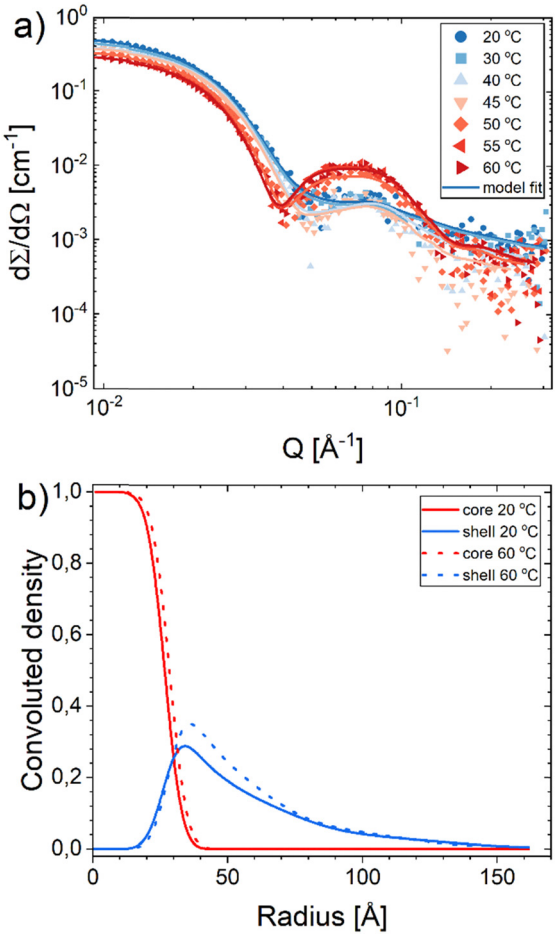

Fig. 3 (a) SAXS curves of C_{28}-PEO3/10 1 : 1 as a function of temperature ranging from 20 °C to 60 °C at 0.5 vol% polymer concentration. Solid lines represent the model fits. Temperature scans of other samples can be found in Fig. S2 and S3 in the ESI.† (b) The density profile of core (red) and shell (blue) as a function of micelle radius of C_{28}-PEO3/10 1 : 1 micelles at 20 °C (solid line) and 60 °C (dotted line).

kinetic factors. When molecular exchange between micelles is rapid (faster than the experimental time scale), thermodynamic control dominates, and the system obtains the energetically most favorable equilibrium structure. Otherwise, so-called kinetically trapped states may occur. Based on our previous kinetic study on C_n-PEO systems,[23] the structure of C_{28}-PEO micelles prepared under the conditions in this work is under thermodynamic control and thus in equilibrium.

As shown in Fig. 4a, the N_{agg} shows a strong dependence on N^*_{PEO} and decreases with increasing N^*_{PEO}. Overall, the observed decrease of N_{agg} can be qualitatively rationalized by a shift of the balance between enthalpic and entropic contributions with the growing corona block. To be specific, the self-assembled micellar structure highly depends on the balance of enthalpic gain of minimizing the area of interfacial contact between the hydrophobic core block and the corona/solvent environment as well as the conformational entropic loss arising from the stretching of the polymer chains when confined into micelles. In other words, the enthalpic gain favors the micellization while the entropic loss counterbalances it. In this case, as PEO length increases, stretching of PEO blocks to a greater extent in the coronal domain impedes the aggregation of the alkyl chains and therefore leads to a smaller aggregation number.

The scaling laws for starlike micelles proposed by Halperin[38] predict that the aggregation behavior should be close to independent of the corona chain length. Apart from a weak logarithmic dependence on the corona-forming chain, the aggregation number solely depends on the core block. The scaling laws, however, assume the limit $N_{corona} \gg N_{core}$, which is not true in our case. Another scaling law and the model taking into account both soluble and insoluble blocks was suggested by Zhulina *et al.*[39] They introduced a weak logarithmic dependence $N_{agg} \propto (\ln N)^{-6/5}$ in the limit of long corona chains. In the literature, it was found that the logarithmic scaling describes well the behavior of micelles with high N^*_{PEO} values,[12] but in our experiment, we observed high deviation for micelles with shorter PEO chains. The prediction is presented in Fig. 4a as a red line. The dependence between N_{agg} and N^*_{PEO} for short PEO chains can be also described with a pseudo mean-field phase approximation proposed by Nagarajan and Ganesh.[40] Our results are in agreement with these theoretical predictions, we observed the scaling of $N_{agg} \propto N^{*-0.53\pm0.06}_{PEO}$. The previous work from Willner *et al.*[41] on a poly(ethylene-propylene)-*block*-poly(ethylene oxide) (PEP-*b*-PEO) micelle system with a fixed PEP core block length showed N_{agg} in the region of N^*_{PEO} larger than 1000 did remain constant as predicted by Halperin. But in the region of N^*_{PEO} ranging from 150 to 750, N_{agg} showed a perfect agreement with the Nagarajan and Ganesh empirical scaling law $N_{agg} \propto N^{*-0.51}_{PEO}$

The core radius R_c as a function of N^*_{PEO} is depicted in Fig. 4b. We can see that R_c decreases with increasing N^*_{PEO}, we observed scaling $R_c \propto N^{*-0.20\pm0.02}_{PEO}$ that is in agreement with $R_c \propto N^{*-0.18}_{PEO}$ predicted by Nagarajan and Ganesh. Note that as the alkyl block is highly hydrophobic, the alkyl core is assumed to be devoid of solvent. According to the theory developed by Tanford,[42] the value of R_c relates to the chain configuration in the core domain. Assuming *n*-alkanes with a fully extended all-*trans* conformation, the maximal possible length can be calculated as

$$l_{C_n,max} = 1.53 + 1.265(n - 1)\ [Å] \quad (14)$$

For C_{28}, $l_{C_{28},max}$ = 35.7 Å. The experimental R_c values of all samples are below this value as shown in Fig. 4b. Obviously, the alkyl blocks did not adopt a fully extended all-*trans* conformation, which is easy to imagine given the spatial confinement in the core domain and the disturbance from kinks along the backbone. Tanford also proposed a flexible conformation of *n*-alkane chains, which is given by ref. 42

$$l_{C_n,flex} = 1.53 + 0.925(n - 1)\ [Å] \quad (15)$$

Thus, $l_{C_{28},flex}$ = 26.5 Å. Comparing R_c with l_{flex} and l_{max} over the examined N^*_{PEO} range unravels that the alkyl blocks adopt a rather flexible conformation when N^*_{PEO} is smaller than 160, while at a larger N^*_{PEO}, a collapsed conformation can be speculated for alkyl blocks. This is in line with the finding that

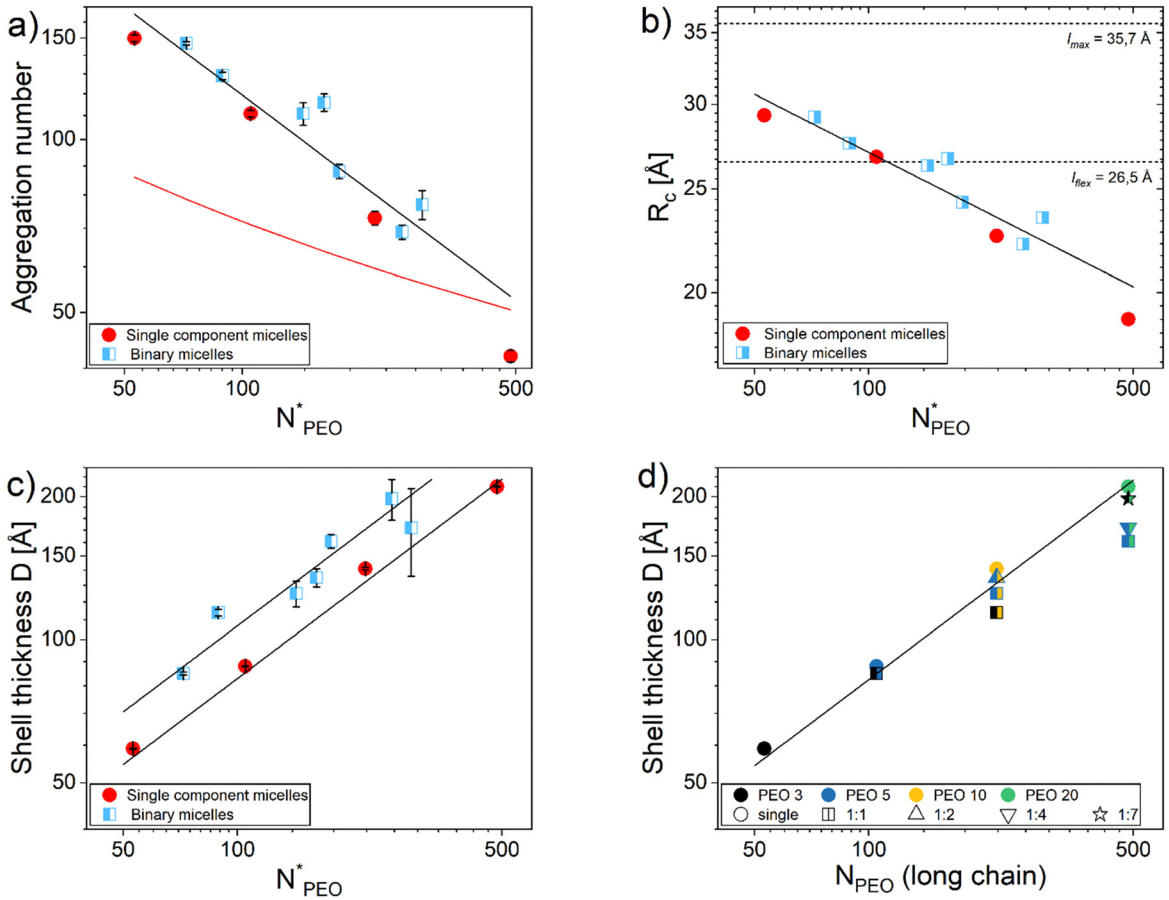

Fig. 4 (a) Aggregation number N_{agg} as a function of the mean PEO block length N^*_{PEO} measured at 20 °C presented in double-logarithmic representation. The black line denotes $N_{agg} \propto N^{*-0.51}_{PEO}$ predicted by Nagarajan & Ganesh, the red line denotes $N_{agg} \propto (\ln N)^{-6/5}$ predicted by Zhulina. (b) Core radius R_c correlation with the mean PEO block length N^*_{PEO} measured at 20 °C presented in double-logarithmic representation. Values of l_{flex} 26.5 Å and l_{max} 35.7 Å indicated with horizontal dash lines were calculated based on the formulas proposed by Tanford. Solid line denotes $R_c \propto N^{*-0.18}_{PEO}$ predicted by Nagarajan & Ganesh, (c) corona thickness D of single-component micelles and binary mixed micelles plotted against the mean PEO block length N^*_{PEO} measured at 20 °C presented in double-logarithmic representation. The lines represent a power-law dependence of $D \propto N^{*3/5}_{PEO}$ for star-like micelle predicted by Halperin, (d) Corona thickness D plotted as a function of the mean PEO block length of the longer micelle component.

the core-related enthalpic contribution to the micellar free energy is less significant for large N^*_{PEO}.

Fig. 4c displays the corona thickness D extracted from SAXS plotted as a function of N^*_{PEO}. Corona thickness shows a power-law dependence on N^*_{PEO} with an exponent of 0.58 ± 0.02 in single-component micelles, which matches the theoretical prediction $D \propto N^{3/5}$ from the scaling theory for the starlike micelle.[38] D values of binary mixed micelles also follow a very similar power law with the exponent 0.53 ± 0.08, but the corona is thicker in comparison to single-component micelles (for the same N^*_{PEO}). That may be explained by the specific structure of mixed micelles where the diameter of the entire micelle depends on the length of the longest PEO chains that are pointing out of the micelle above the shorter ones. Addition of shorter PEO decreases N^*_{PEO} but doesn't change significantly outer radius of micelle. Corona thickness as a function of longer component of the micelles is presented in Fig. 4d. As a result, outer shell has lower PEO fration than single component micelles. We could observe the phenomenon in our system, samples C_{28}-PEO3/5 1 : 1 and C_{28}-PEO5 have the same outer radius, whereas pairs of C_{28}-PEO5/10 1 : 1 & C_{28}-PEO10 and C_{28}-PEO3/20 1 : 7 & C_{28}-PEO20 have very similar outer radii.

3.4 Melting-freezing transition in the alkyl core

Density as a function of the temperature of C_{28}-PEOx mixed or pure micelles is shown in Fig. 5a. The curves are arranged in the graph in order of the decreasing mean length of the PEO block from top to bottom. It should be pointed out that the density transition is becoming progressively weaker at larger N^*_{PEO} is due to a lower mass fraction of the alkyl block in the whole copolymer at a fixed polymer concentration. There is a clear hint of discontinuity in polymer density upon heating, which indicates an abrupt decrease in the density of alkyl blocks since PEO homopolymer does not exhibit any discontinuity (Fig. S4, ESI†). This discontinuity confirms again the first-order phase transition of the alkyl blocks. As shown in Fig. 5a, the transition temperature slowly shifts towards a lower value with increasing N^*_{PEO}. The results of molar heat capacity C_p

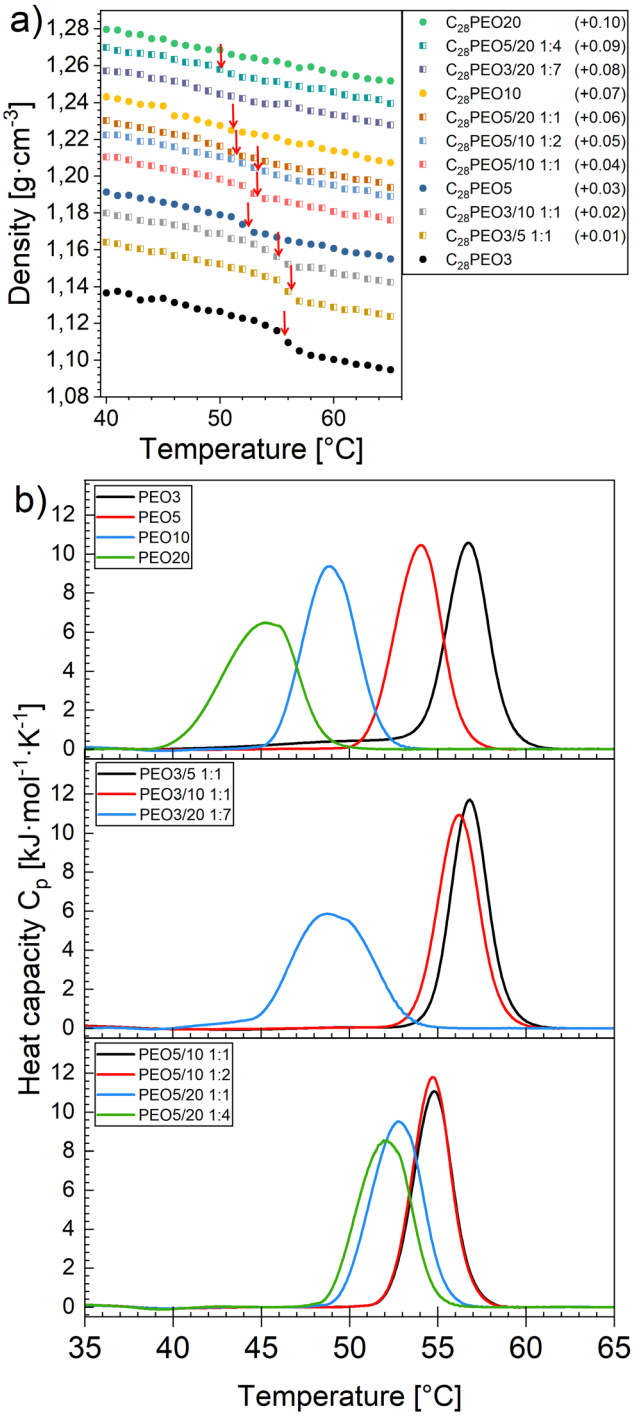

Fig. 5 (a) Density of the polymeric micelles ρ_{pol} as a function of temperature T in the temperature range 40–65 °C. From top to bottom, N^*_{PEO} decreases from 485 to 53. To avoid overlapping, offset of 0.01 was applied between each dataset, final offset value is indicated in the legend. Red arrows indicate melting of semicrystalline core, (b) Temperature dependence of molar heat capacity C_p measured by DSC heating run at a heating scan rate of 2 °C min^{-1}.

from DSC endothermic measurements are shown in Fig. 5b (heating) and Fig. S5 (ESI†) (cooling). The melting point T_m of the alkyl blocks determined through the peak of the derivative of the density and melting/freezing point T_m/T_f determined from the DSC peak temperature are plotted in Fig. 6a, whereas the values of corresponding enthalpies $\Delta H_m/\Delta H_f$ are plotted in Fig. 6b. It is worth noting that the micelle samples from polymer mixtures only exhibit a single melting transition upon heating in both density and DSC measurements, strengthening the hypothesis of the formation of mixed micelles rather than two separate populations of single-component micelles. The DSC curve of C_{28}-PEO3/20 1 : 7, which displays well-separated peaks for the pure micelles of each component (centered at 57 °C and 45 °C, respectively), exhibits a single peak at 49 °C. This finding provides compelling evidence in support of the formation of mixed micelles. We observed a broadening of the peak of C_{28}-PEO20 in both the heating and cooling runs. This effect is indicative of a decrease in the domain size and a larger surface-to-volume ratio, which result in a smaller degree of cooperativity of the liquid. A similar effect has been previously observed for water,[43] alkanes,[44] and in our earlier publication.[29] As evidenced by extant literature, tightly packed PEO chains have the potential to crystallize even when dissolved in a solvent. In a previous experiment, analyzing the structure of C_{28}-PEO micelles,[32] the presence of a very thin (less than 1 nm) dry layer of PEO coating the hydrophobic C_{28} micellar core was proved using a combination of NMR, SAXS and SANS. The effect is only discernible by employing contrast variation SANS to isolate the core scattering. However, no heat flow consistent with ordered PEO was identified by DSC. This may indicate that either the layer is amorphous or the contribution to the measured signal is simply too small.

In our system, the melting and freezing enthalpies decrease with increasing N^*_{PEO} (Fig. 6b). The decrease in enthalpy reflects a decreasing packing order or crystallinity χ_c. In general, the crystallinity can be estimated on the basis that the melting enthalpy is proportional to crystallinity.[45] Therefore, we can qualitatively know that χ_c of C_{28} blocks in C_{28}-PEOx micelles decreases as N^*_{PEO} increases from the monotonous decrease trend of the ΔH_m *vs.* N^*_{PEO} curve in Fig. 6b. The crystallinity χ_c is calculated by dividing the melting enthalpy of the alkyl core by that of the fully crystallized bulk C_{28} alkane/octacosane (100.0 kJ mol^{-1}),[46] yielding χ_c between 36% and 31%.

The relatively low χ_c compared to the bulk alkane undoubtedly correlates with the confinement of alkyl blocks in the micellar core of merely a few nanometers in radius. Given that R_c is inversely proportional to N^*_{PEO} as demonstrated above, we know that χ_c is proportional to R_c. It can be intuitively understood by imagining the difficulty of molecular chain packing within a curved nanodomain. The smaller the R_c, the higher the curvature, and consequently the greater the difficulty to pack in a crystalline state. Additionally, in this self-confined micellar system, one chain-end of the alkyl block is tethered to the core–corona interface as a result of the covalent binding with the PEO corona block, which gives rise to the moderate restriction on chain mobility and consequently a reduction in the χ_c.[47,48] In a previous study,[32] which involved extended nuclear magnetic resonance (NMR) analysis, it was found that above the melting transition, the core blocks of the C_n-PEO micellar system were liquid-like, with low but finite orientational order,

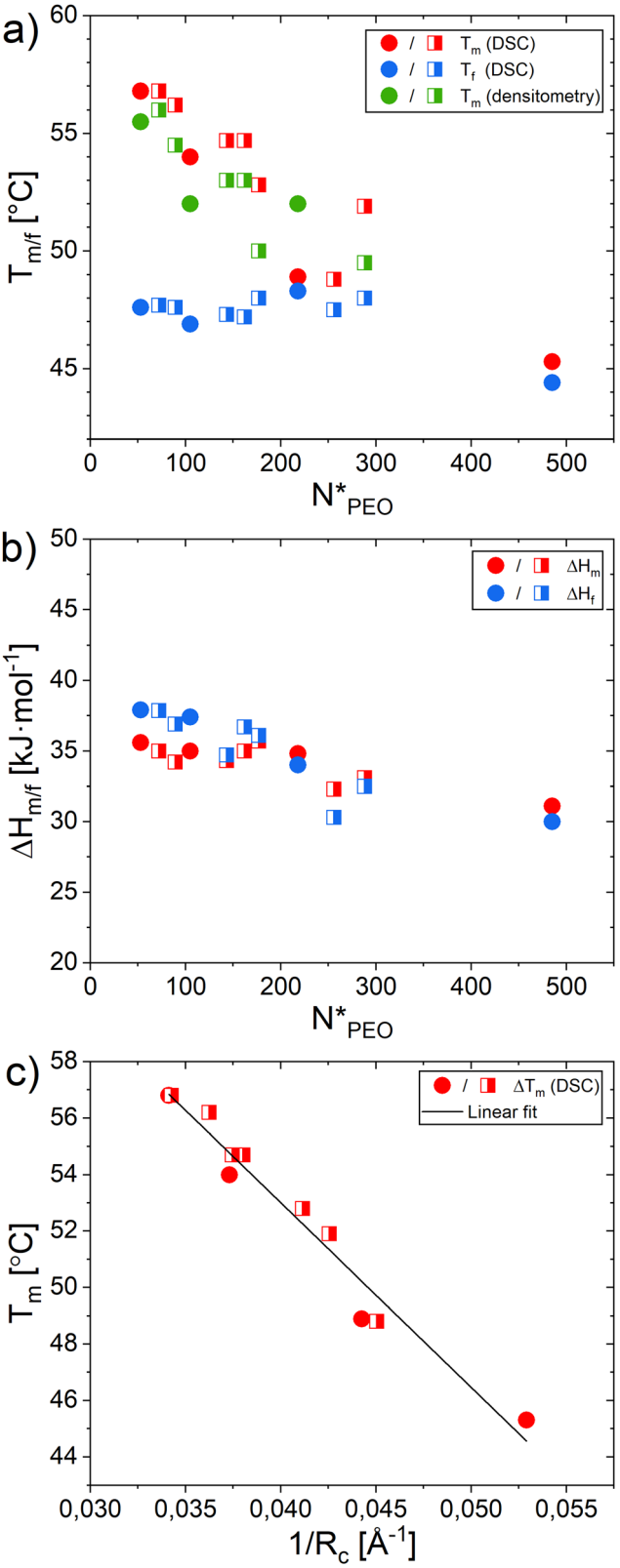

Fig. 6 (a) Melting/freezing points T_m/T_f determined from DSC as well as T_m from densitometry plotted against the mean PEO block length N^*_{PEO}, (b) melting/freezing enthalpies $\Delta H_m/\Delta H_f$ determined from DSC plotted against the mean PEO block length N^*_{PEO}, (c) Melting temperature of the C_{28} alkyl core blocks plotted against the inverse core radius $\frac{1}{R_c}$. The solid line is a linear fit with a coefficient of determination R^2 of 0.96.

in agreement with the persistent asphericity of the core. However, in the region below the melting transition, the system displayed remarkably elevated relaxation rates, suggesting the presence of a rotator-like phase characterized by predominantly all-*trans* chain conformation and reorientations occurring within the range of milliseconds to microseconds. Studies on micellar systems from other diblock copolymers like poly(ε-caprolactone)-*b*-poly(ethylene oxide),[49] polymethylene-*b*-poly(acrylic acid)[50] and polystyrene-*b*-poly(4-vinylpyridine)[51] have provided more examples on confinement effects.

T_m shifts 12 °C towards a lower temperature with an increase in N^*_{PEO} (Fig. 6a). It has been fairly well documented that the T_m depression in the confined domain is associated with the finite size effect, termed as the Gibbs–Thomson effect.[52,53] We know that the surface-to-volume ratio of the material is greatly enhanced upon nanoconfinement. The effect stems from the excess energy of the formation of the surface. Our previous studies[23,29] on other C_n-PEO micellar systems have revealed a melting point depression ΔT_m proportional to the inverse of R_c, which could be described by the generalized Gibbs–Thomson equation

$$\Delta T_m = T_m^0 - T_m = \frac{\alpha\gamma V_{C_n} T_m^0}{R_c \Delta H_m} \quad (16)$$

where T_m^0 is the melting point of the bulk *n*-alkane, α is a prefactor characteristic for the confinement geometry, γ is the interfacial tension, V_{C_n} is the molar volume of the *n*-alkyl, and ΔH_m is the bulk melting enthalpy. In this work, because the alkyl block length is kept constant and micellar cores of all the examined micelles can be considered as being spherical, the terms ΔH_m, V_{C_n}, T_m^0, γ and α on the right-hand side of the equation are constant. Thus, the melting temperatures T_m obtained from DSC are plotted as a function of the reciprocal core radius $\frac{1}{R_c}$ as shown in Fig. 6c. It should be mentioned that the apparent degree of crystallinity is rather low suggesting partially crystalline core chains and that the core radius is not necessarily the right measure of the domains. However, an apparent low value of χ_c from DSC, which is essentially a measure of mobility might be affected by other effects. First, our earlier combined NMR and SANS investigations have indicated that the core is in an ordered "rotator phase" rather than a monoclinic phase.[32] This would imply that the reference enthalpy of fusion is not that of the fully crystalline bulk phase. Secondly, the self-assembly and connectivity to the PEO might increase mobility such that the measured enthalpy of fusion is lowered. Thus, it is likely that the core radius represents the domain size. We can see that data set from both the pure micelles and the mixed micelle nicely follow the trend expected from the Gibbs–Thomson equation. Extrapolation of the graph to $\frac{1}{R_c} = 0$ corresponds to the infinite R_c and T_m^0 of the bulk material. We find the value of T_m^0 = 79 °C that is close to melting temperature of 1-octacosanol (T_m = 83 °C),[54] which is the precursor polymerized to yield C_{28}PEO. In a published work reporting on fully crystallized polymer samples, extrapolation of the melting line to the infinitely large domain (bulk, where $R_c^{-1} = 0$) do indeed yield the expected T_m^0 as expected from the Gibbs–Thomson equation.[55,56]

The freezing points determined by the molar heat capacity-temperature curves from the DSC cooling run (Fig. S5, ESI†) show a small shift to a lower temperature from 48 to 44.5 °C upon increasing N^*_{PEO} (Fig. 6a). T_f is always lower than T_m as shown in Fig. 6a, termed as undercooling, which is in line with a well-known fact that freezing typically takes place at a lower temperature than melting as a result of the kinetic barrier associated with the formation of nuclei for crystallization.[57] Additionally, in this scenario, nanodomains are spatially too small to place any macroscopic impurities to act as nuclei. Thus, the nucleation mechanism undoubtedly switches from heterogeneous nucleation (usually for the bulk macromolecules) to surface or homogeneous nucleation.[58] For instance, a dramatic decrease in T_f of the poly(ε-caprolactone) (PCL) core blocks from 28 °C to −17 °C has been documented for micelles self-assembled from PCL-*b*-PEO copolymers compared with the bulk PCL, while the T_m of PCL cores was *ca.* 54 °C, which the authors considered as surface nucleation.[49] In another study, where homogenous nucleation of *n*-alkanes was investigated, the difference between T_m and T_f of pure *n*-$C_{28}H_{58}$ was equal 14 °C.[59] Considering the relatively small differences between T_m and T_f of the alkyl core observed in this work, *i.e.*, low undercooling effect, surface nucleation mechanism is the more likely mechanism.[58] It should be pointed out that the core radii in the current system are one order of magnitude smaller than those in the publication of Mai *et al.*[49] Interestingly, the gap between T_m and T_f is narrowing with N^*_{PEO} and almost closes at $N^*_{PEO} = 485$ (the corresponding R_c = 19 Å). As illustrated in Fig. 4a, N_{agg} monotonously decreases with increasing N^*_{PEO}, *i.e.*, thus, there are fewer alkyl chains in the core. It may become easier to arrange in an ordered manner in the case of fewer alkyl chains as the overall degree of freedom of the chains in one core is smaller.

4. Conclusion

In summary, we have investigated the structure of mixed micelles formed in water from binary C_{28}-PEO*x* mixtures with different PEO corona block lengths N^*_{PEO} at a polymer volume fraction of 0.25 vol% by SAXS. The micelles were prepared by a co-solvent approach. The SAXS profiles of the tested samples exhibited typical features of spherical core–shell micelles and could be perfectly fitted by a spherical core-dual shell model. Decrease of N_{agg} and R_c were observed with increasing the mean corona block length. The N_{agg} scaled as $N_{agg} \propto N^{*-0.53\pm0.06}_{PEO}$, which is consistent with the theoretical prediction of $N_{agg} \propto N^{*-0.51}_{PEO}$. A closer inspection of radial density profiles revealed that in micelles with the same outer radius, mixed micelles are characterized by higher density at the core–shell interface and lower at the shell–solvent interface in comparison to one-component micelles, which suggests more stretched PEG conformation in case of one-component micelles.

One single-phase transition of the alkyl core from binary polymer mixtures was observed upon heating in both the density and DSC measurements, confirming the formation of mixed micelles. Calculations based on melting enthalpy data from DSC revealed that the apparent crystallinity of the alkyl core decreased from 36% to 31% as the N^*_{PEO} increased from 53 to 485. However, as was found in our earlier work,[32] the ordered phase in the confined core resembles more a ''rotator phase'' rather than a monoclinic phase typical for *n*-octacosane at low temperature.[60] Interestingly we found that the melting point could be modulated and finely tuned through co-assembly of polymers with different PEO length. T_m decreased with an increase in N^*_{PEO} and the reduction with respect to the bulk C_{28} alkane was proportional to $\frac{1}{R_c}$, as predicted by the Gibbs–Thomson equation. The work thus shows how confinement effects induced by self-assembly play an important role in determining the phase behaviour of micelles which may be of importance *e.g.* applications for solubilization of drug delivery. This study not only provides important insight into the basic physical chemistry, but also shows how the nature of the core in micellar systems can be manipulated by simple co-assembly strategies, either with the shell block length as shown in this work or using binary core block lengths as a previous work.[19]

Author contributions

Szymon M. Szostak: data curation, formal analysis, investigation, validation, visualization, Nico König: formal analysis, investigation, software Lutz Willner: conceptualization, methodology, resources, supervision, Reidar Lund: conceptualization, data curation, methodology, project administration, software, resources, supervision, funding aquistion, all authors: writing – review and editing.

Data availability

Small angle X-ray scattering data for this article, are available at European Synchrotron Radiation Facility repository at **https://doi.org/10.15151/ESRF-ES-1602273227**. The data supporting this article have been included as part of the ESI.†

Conflicts of interest

There are no conflicts to declare.

Acknowledgements

We indebted to Dr Shanshan Chen (Sun Yat-sen University) for the preliminary study and report. We are grateful the Norwegian Research Council (Project No. 315666, RL). We kindly acknowledge the provision of SAXS beamtime at BM29 at ESRF (Grenoble, France) and thank Dr Petra Pernot and the PSCM lab for support during the SAXS experiment. We also acknowledge the Norwegian national infrastructure for X-ray diffraction and scattering (RECX) at the University of Oslo (Norway) for SAXS beamtime. We would like to thank Bente A. Breiby (Department of Pharmacy, University of Oslo) for performing the nanoDSC experiments.

References

1 K. Letchford and H. Burt, *Eur. J. Pharm. Biopharm.*, 2007, **65**, 259–269.
2 U. Tritschler, S. Pearce, J. Gwyther, G. R. Whittell and I. Manners, *Macromolecules*, 2017, **50**, 3439–3463.
3 A. Rösler, G. W. M. Vandermeulen and H. A. Klok, *Adv. Drug Delivery Rev.*, 2012, **64**, 270–279.
4 A. M. Bodratti and P. Alexandridis, *Expert Opin. Drug Delivery*, 2018, **15**, 1085–1104.
5 F. Xu, H. Li, Y. L. Luo and W. Tang, *ACS Appl. Mater. Interfaces*, 2017, **9**, 5181–5192.
6 C. Li, C. C. Tho, D. Galaktionova, X. Chen, P. Král and U. Mirsaidov, *Nanoscale*, 2019, **11**, 2299–2305.
7 K. Liu, X. Wang, X. Li-Blatter, M. Wolf and P. Hunziker, *ACS Appl. Bio Mater.*, 2020, **3**, 6919–6931.
8 R. Lund, L. Willner and D. Richter, *Adv. Polym. Sci.*, 2013, **259**, 51–158.
9 T. Li, A. J. Senesi and B. Lee, *Chem. Rev.*, 2016, **116**, 11128–11180.
10 X. Ye, Z. W. Li, Z. Y. Sun and B. Khomami, *ACS Nano*, 2016, **10**, 5199–5203.
11 R. S. Tu and M. Tirrell, *Adv. Drug Delivery Rev.*, 2004, **56**, 1537–1563.
12 T. Zinn, L. Willner, R. Lund, V. Pipich, M. S. Appavou and D. Richter, *Soft Matter*, 2014, **10**, 5212–5220.
13 A. B. Ebrahim Attia, Z. Y. Ong, J. L. Hedrick, P. P. Lee, P. L. R. Ee, P. T. Hammond and Y. Y. Yang, *Curr. Opin. Colloid Interface Sci.*, 2011, **16**, 182–194.
14 A. P. Lindsay, R. M. Lewis, B. Lee, A. J. Peterson, T. P. Lodge and F. S. Bates, *ACS Macro Lett.*, 2020, **9**, 197–203.
15 K. T. Oh, T. K. Bronich and A. V. Kabanov, *J. Controlled Release*, 2004, **94**, 411–422.
16 D. Zhao, Y. Ma, E. Wang and T. P. Lodge, *Macromolecules*, 2019, **52**, 4729–4738.
17 Y. Sun, R. Tan, Z. Ma, D. Zhou, J. Li, D. Kong and X. H. Dong, *Giant*, 2020, **4**, 100037.
18 Y. Sun, R. Tan, Z. Ma, Z. Gan, G. Li, D. Zhou, Y. Shao, W. Bin Zhang, R. Zhang and X. H. Dong, *ACS Cent. Sci.*, 2020, **6**, 1386–1393.
19 N. König, L. Willner and R. Lund, *Soft Matter*, 2019, **15**, 7777–7786.
20 Z. X. Du, J. T. Xu and Z. Q. Fan, *Macromolecules*, 2007, **40**, 7633–7637.
21 C. Secker, A. Völkel, B. Tiersch, J. Koetz and H. Schlaad, *Macromolecules*, 2016, **49**, 979–985.
22 T. Zinn, L. Willner, V. Pipich, D. Richter and R. Lund, *ACS Macro Lett.*, 2015, **4**, 651–655.
23 N. König, L. Willner, V. Pipich, T. Zinn and R. Lund, *Phys. Rev. Lett.*, 2019, **122**, 078001.
24 X. Zhuo, T. Lei, L. Miao, W. Chu, X. Li, L. Luo, J. Gou, Y. Zhang, T. Yin, H. He and X. Tang, *J. Colloid Interface Sci.*, 2018, **529**, 34–43.
25 J. Dai, Z. Alaei, B. Plazzotta, J. S. Pedersen and I. Furó, *J. Phys. Chem. B*, 2017, **121**, 10353–10363.
26 Y. Deng, J. Ling and M. H. Li, *Nanoscale*, 2018, **10**, 6781–6800.
27 A. L. Glover, S. M. Nikles, J. A. Nikles, C. S. Brazel and D. E. Nikles, *Langmuir*, 2012, **28**, 10653–10660.
28 O. R. Monaghan, P. H. H. Bomans, N. A. J. M. Sommerdijk and S. J. Holder, *Polym. Chem.*, 2017, **8**, 5303–5316.
29 T. Zinn, L. Willner and R. Lund, *Phys. Rev. Lett.*, 2014, **113**, 238305.
30 M. Alcoutlabi and G. B. McKenna, *J. Phys.: Condens. Matter*, 2005, **17**, R461.
31 M. D. Tully, J. Kieffer, M. E. Brennich, R. Cohen Aberdam, J. B. Florial, S. Hutin, M. Oscarsson, A. Beteva, A. Popov, D. Moussaoui, P. Theveneau, G. Papp, J. Gigmes, F. Cipriani, A. Mccarthy, C. Zubieta, C. Mueller-Dieckmann, G. Leonard and P. Pernot, *J. Synchrotron Radiat.*, 2023, **30**, 258–266.
32 N. König, L. Willner, G. Carlström, T. Zinn, K. D. Knudsen, F. Rise, D. Topgaard and R. Lund, *Macromolecules*, 2020, **53**, 10686–10698.
33 C. Svaneborg and J. S. Pedersen, *Phys. Rev. E*, 2001, **64**, 010802.
34 J. S. Pedersen and C. Svaneborg, *Curr. Opin. Colloid Interface Sci.*, 2002, **7**, 158–166.
35 D. J. Kinning and E. L. Thomas, *Macromolecules*, 1984, **17**, 1712–1718.
36 B. Plazzotta, J. Dai, M. A. Behrens, I. Furó and J. S. Pedersen, *J. Phys. Chem. B*, 2015, **119**, 10798–10806.
37 M. Vuorte, J. Määttä and M. Sammalkorpi, *J. Phys. Chem. B*, 2018, **122**, 4851–4860.
38 A. Halperin, *Macromolecules*, 1987, **20**, 2943–2946.
39 E. B. Zhulina, M. Adam, I. Larue, S. S. Sheiko and M. Rubinstein, *Macromolecules*, 2005, **38**, 5330–5351.
40 R. Nagarajan and K. Ganesh, *J. Chem. Phys.*, 1989, **90**, 5843–5856.
41 L. Willner, A. Poppe, J. Allgaier, M. Monkenbusch, P. Lindner and D. Richter, *Europhys. Lett.*, 2000, **51**, 628.
42 C. Tanford, *The hydrophobic effect: formation of micelles and biological membranes*, J. Wiley, 2nd edn, 1980.
43 S. Jähnert, F. Vaca Chávez, G. E. Schaumann, A. Schreiber, M. Schönhoff and G. H. Findenegg, *Phys. Chem. Chem. Phys.*, 2008, **10**, 6039–6051.
44 D. Wang, Y. Dong, W. Sun, N. Lu and X. Lan, *Chem. Thermodyn. Therm. Anal.*, 2021, **3–4**, 100019.
45 R. J. Young and P. A. Lovell, *Introd. to Polym.*, 3rd edn, 2011, pp. 1–653.
46 U. Domanska and D. Wyrzykowska-Stankiewicz, *Thermochim. Acta*, 1991, **179**, 265–271.
47 S. Nakagawa, H. Marubayashi and S. Nojima, *Eur. Polym. J.*, 2015, **70**, 262–275.
48 S. Nojima, Y. Ohguma, K. I. Kadena, T. Ishizone, Y. Iwasaki and K. Yamaguchi, *Macromolecules*, 2010, **43**, 3916–3923.
49 B. Mai, Z. Li, R. Liu, S. Feng, Q. Wu, G. Liang, H. Gao and F. Zhu, *J. Polym. Res.*, 2013, **20**, 1–8.
50 H. C. Lu, Y. Xue, Q. L. Zhao, J. Huang, S. G. Xu, S. K. Cao and Z. Ma, *J. Polym. Sci., Part A: Polym. Chem.*, 2012, **50**, 3641–3647.
51 C. Göbel, C. Hils, M. Drechsler, D. Baabe, A. Greiner, H. Schmalz and B. Weber, *Angew. Chem., Int. Ed.*, 2020, **59**, 5765–5770.
52 M. Perez, *Scr. Mater.*, 2005, **52**, 709–712.

53 S. Sen, S. H. Risbud and M. H. Bartl, *Acc. Chem. Res.*, 2020, **53**, 2869–2878.
54 L. Martínez, E. Uribarri and A. Laguna, *Arch. Pharm. Pharm. Med. Chem.*, 1999, **332**, 439–441.
55 G. Strobl, *Prog. Polym. Sci.*, 2006, **31**, 398–442.
56 P. H. Chen, S. J. Lin, J. C. Tsai, U. S. Jeng and A. C. Su, *Macromolecules*, 2020, **53**, 3059–3070.
57 F. C. Meldrum and C. O'Shaughnessy, *Adv. Mater.*, 2020, **32**, 2001068.
58 R. M. Michell, I. Blaszczyk-Lezak, C. Mijangos and A. J. Müller, *Polymer*, 2013, **54**, 4059–4077.
59 M. J. Oliver and P. D. Calvert, *J. Cryst. Growth*, 1975, **30**, 343–351.
60 X. Wang, Y. Wei, D. Zhang, X. Lan, F. Han and X. Z. Lan, *Thermochim. Acta*, 2020, **690**, 178687.

